Formation of Fine Bubbles by Plasma in Water

T. Sato[1], S. Uehara[1], R. Kumagai[1], T. Miyahara[2], M. Oizumi[1], T. Nakatani[3], S. Ochiai[1], T. Miyazaki[1], H. Fujita[1], S. Kanazawa[4], K. Ohtani[1], A. Komiya[1], T. Kaneko[1], T. Nakajima[1], M. Tinguely[5], and M. Farhat[5]
[1]Tohoku University, 2-1-1 Katahira, Aoba-ku, Sendai 980-8577, Japan
[2]Shizuoka University, 3-5-1 Johoku, Naka-ku, Hamamatsu 432-8561, Japan
[3]Okayama University of Science, 1-1 Ridaichou, Kita-ku, Okayama 700-0005, Japan
[4]Oita University, 700 Dannoharu, Oita 870-1192, Japan
[5]EPFL, Avenue de Cour 33 bis, 1007 Lausanne, Switzerland

Abstract— Plasma in water is capable of forming bubbles because streamer gas channels formed by the discharge show the same process of cavitation bubble dynamics, such as growth, shrink, collapse, rebound, and fragmentation. This paper introduces the formation of fine/ultrafine bubbles, generation of hydrogen gas in bubbles, an estimation of the amount of electrical charge in bubbles, and a method for distinguishing gas bubbles from solid particles.

Keywords—Streamer, electrical charges, discharge in water, nano/micro-meter scale bubbles

I. Introduction

Formation of fine bubbles in liquids has been studied extensively. For example, bubble formation occurs in blood due to a decrease in pressure, causing decompression sickness [1], and in magma due to a wide range of pressure and temperatures [2]. In the industrial field, it is known that the collapse of cavitation bubbles results in erosion of hydraulic machines, and causes a decrease in efficiency of some hydraulic equipment, such as pumps and propellers [3].

Methods of fine bubble formation include those that use a flowing liquid (venturi, ejector, rotary liquid flow), those that use a pressurization and decompression, those that do not use a flowing liquid (porous membrane, electrolysis and rotary gas flow), those that use a polymer (emulsion solvent vaporization, cross linking polymerization and atomization-reconstitution), and those that use a type of low power generation (breakdown and organic membrane) [4].

The single cavitation bubble generated by a laser or spark has been used to clarify bubble dynamics [5,6]. Theoretical studies based on Rayleigh's theory have also been performed and have clarified that the initial collapsing process corresponds to the Rayleigh–Plesset model, and that rebounds occur after the initial bubble collapses. The rebounds become smaller, and the bubble disappears or becomes stable in the last stage. These results suggest the generation of microbubbles after the collapse of a bubble. It is also known that the hot spot generated at the initial stage by the spark or the laser becomes plasma, because the temperature reaches 10,000 to 20,000 K [6]. A thermal dissociation of the water occurs when the plasma is generated, implying that non-condensable gases are generated by chemical reactions among dissociated atoms and molecules. However, the effect of chemical reactions on microbubble generation after the collapse of the bubbles has not been clarified in either the case of the laser or the spark. Plasma in water [7] has been recently applied to many applications, such as water treatments [8], sterilization [9], medical treatments [10,11], material processes [12], and agriculture treatments [13], as it can easily generate chemically active species, ultraviolet radiation, heat, shock waves, and fine bubbles [7,14,15].

We have been investigating the formation of fine/ultrafine bubbles using plasma in water. In this review, we introduce how fine/ultrafine bubbles are formed by plasma in water, the kind of non-condensable gas included in the bubbles, how the bubbles are observed, and a method to distinguish between gas bubbles and solid particles.

II. Formation of Fine Bubbles

Fig. 1 shows the experimental setup. Plasma was generated at the tip of a tungsten electrode with the curvature radius of 0.03 mm, which was covered with silicone except for the end face of the electrode.

An electrically insulated and ring-shaped grounded copper wire electrode was installed at the bottom of a cell filled with ultrapure water. A high voltage was applied to the wire electrode, which was covered by a ceramic tube and silicone except for the end face. A wire ground electrode was set at the bottom of the cuvette.

Fig. 2 (a) shows the plasma-generated fine bubbles with applying a positive pulse voltage of 6 kV_{0p}. The bubbles were generated at the tip of a needle electrode. In 100 ms, the bubble jet was generated from the tip of the powered electrode. The bubbles expanded and the whole vessel was filled with small bubbles at t = 20 s. After the plasma generation was stopped,

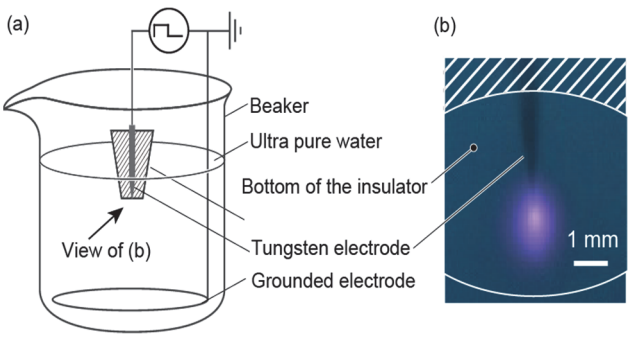

Fig. 1. (a) Experimental setup and (b) photograph of the plasma emission.

Corresponding author: Takehiko Sato
e-mail address: sato@ifs.tohoku.ac.jp

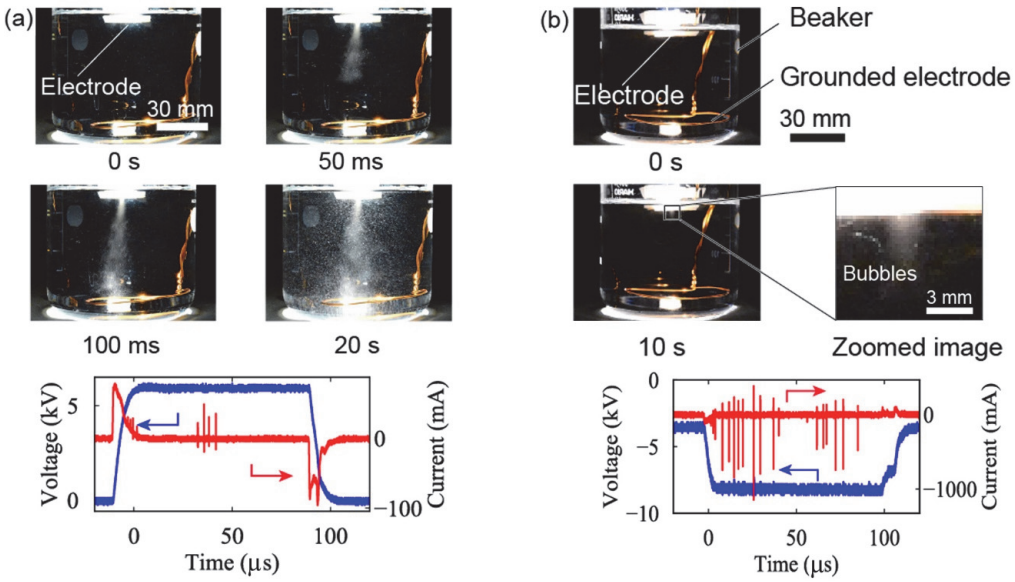

Fig. 2. Photographs and waveforms of the voltage and current for the generation of fine bubbles in the cases of (a) the positive applied voltage of 6 kV_{0p} and (b) the negative applied voltage of -3.5 to -5.5 kV. The time below the photograph denote the discharge time.

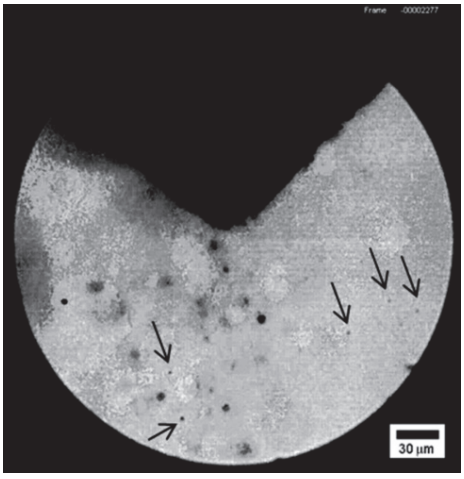

Fig. 3. Photographs of plasma-generated bubbles. Arrowed bubbles are less than 5 μm. [17]

TABLE I
AVERAGE DIAMETER OF THE PLASMA-GENERATED ULTRAFINE BUBBLES

Condition	Control	Voltage application only	Plasma	Plasma
Diameter (nm)	NA	455	132	164
Standard deviation of diameter (nm)	NA	130	3	37
Number of samples	3	3	3	25
Instrument model	DLS-6500	DLS-6500	DLS-6500	NANO FOX

then the bubbles started to rise and disappear immediately. Fig. 2 (b) shows the plasma-generated fine bubbles with applying a negative voltage of -5.5 kV to -3.5 kV. The amount of generated bubble and the diameter is much smaller than the case of positive voltage. Although visible bubbles were not observed, fine bubbles of less than 5 μm, which are invisible to the naked eye, still remained in the water, as shown in Fig. 3 [17].

Table I shows the average diameter of the ultrafine bubbles that were analyzed by dynamic light scattering devices (Otsuka Electronic, DLS-6500 and Sympatec, NANOFOX) in the case of maximum and minimum applied voltages of –5.5 and –3.5 kV, respectively, with a frequency of 10 kHz. Because bubbles on the micro-meter scale rise and disappear owing to buoyancy, the bubbles on the nano-meter scale of ~150 nm remain in the water in the case of plasma generation. In the case of the voltage application only, the average diameter of the bubbles was 455 nm because of electrolysis. This implies that bubble size increases if electrolysis occurs. The devices were not able to detect any bubbles in the cases where a voltage was not applied. This result shows that stable ultrafine bubbles can probably be generated by using plasma in water [16].

III. GROWTH AND COLLAPSE OF STREAMER CHANNEL

Figs. 4 and 5 show a series of shadowgraph images of the positive and negative streamer propagations and collapse processes, respectively. The positive streamer was generated at the tip of the needle electrode that was set in the quartz cuvette (10 × 10 × 45 mm) filled with pure water when a high voltage of +14 kV was applied. A grounded wire electrode was located at a gap of 2 mm from the tip of the needle electrode. The frame rate of the camera was 10 Mfps with an exposure time of 50 ns.

At t = 3.0 μs, a protrusion was formed at the tip of the bubble cluster and the streamer started to propagate after 0.1

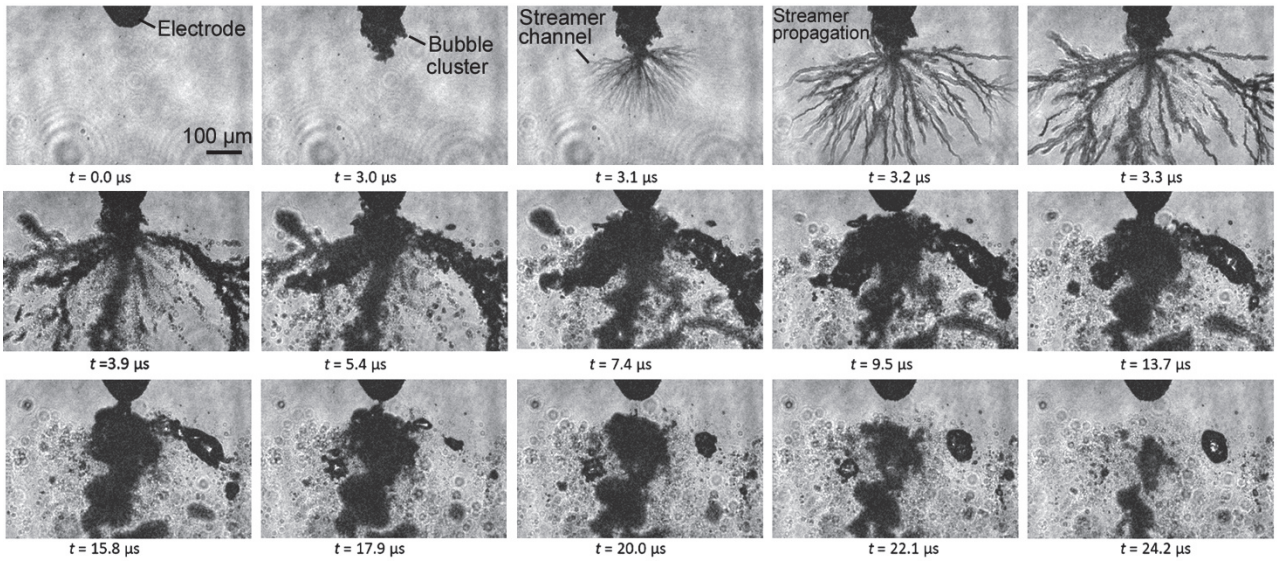

Fig. 4. Series of shadowgraph images of positive streamer propagation, growth of streamer gas channels, shrink and collapse of the gas channels, and formation of fine bubbles.

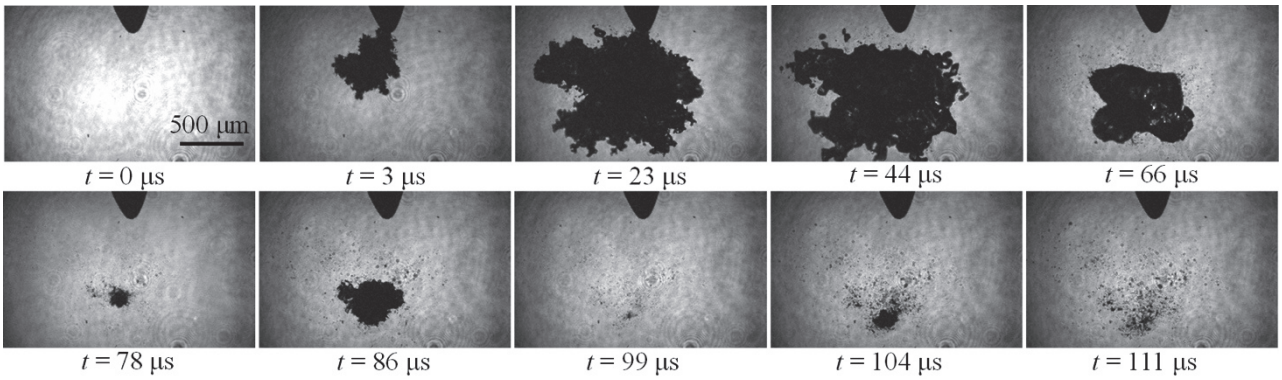

Fig. 5. Series of shadowgraph images of growth and collapse of negative streamer gas channels and the formation process of fine bubbles.

μs. Numerous filamentary streamer channels were generated and propagated semi-spherically. Inception and propagation of the positive streamer in highly spatial temporal resolution are reported in the references [18-21]. After the propagation of streamers stopped at t = 3.3 μs, the gas channels expanded because most of the gas in the channels was water vapor generated by the heat of discharges. The gas channel expanded to a maximum size at t = 7.4 μs, then it started to shrink. Finally, fine bubbles were formed after they separated, collapsed, and rebounded.

The negative streamer propagated with a coralline-like shape, rather than a filament-like shape, under the same condition as the positive case, except that the applied voltage was –23 kV. The streamer expanded with an appearance of pulsed currents and exhibited a maximum area at t = 23 μs. Then, the streamer channels started to shrink and collapsed at t = 78 μs. Finally, fine bubbles remained after rebounds.

As shown in Fig. 2, the amount of generated fine bubbles in the case of positive polarity is much greater than that of the negative polarity. This is probably caused by the different shapes of the streamers, because the positive streamer was fragmented into several bubbles when it was collapsed. On the other hand, the negative streamer seemed to collapse as one bubble. However, the ultrafine bubbles shown in Table I was observed in the case of the negative polarity, however ultrafine bubbles were not observed in the case of the positive polarity. This result suggests that the bubbles generated by the negative polarity might be ultrafine bubbles which are invisible by naked eyes.

These results show that the fine/ultrafine bubbles can be generated by collapse of streamer gas channels.

IV. Charge Estimation of Plasma Fine Bubbles

The charge at the interface of the bubble is considered to increase stability of bubbles and a zeta potential is known as representative of the amount of charge of the bubble. It is reported that: (1) there is no relation between the zeta potential and bubble diameter, (2) the zeta potential of microbubbles is affected by pH, and (3) the zeta potential of a microbubble is negative [4]. We have succeeded in estimating the amount of charge of plasma fine bubbles using their movements under a static electric field.

Fig. 6 shows the moving traces of the residual bubbles under the electric field. The bubbles move along the electric line of force with an average velocity of 17 m/s and a

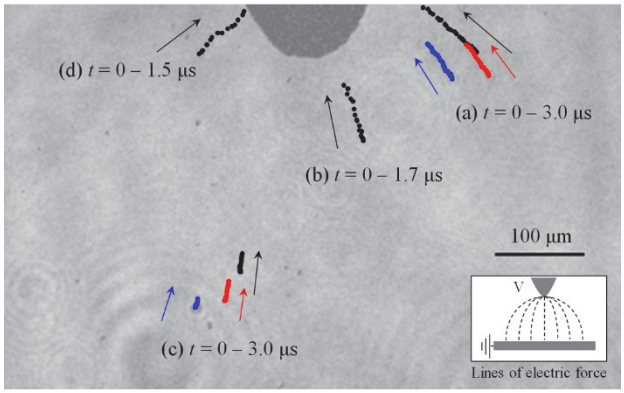

Fig. 6. Moving traces of the residual bubbles. The periods of the traces are (a) t = 0–3.0 μs, (b) t = 0–1.7 μs, (c) t = 0–3.0 μs, (d) t = 0–1.5 μs. The time resolution of the bubble movement is 0.1 μs.

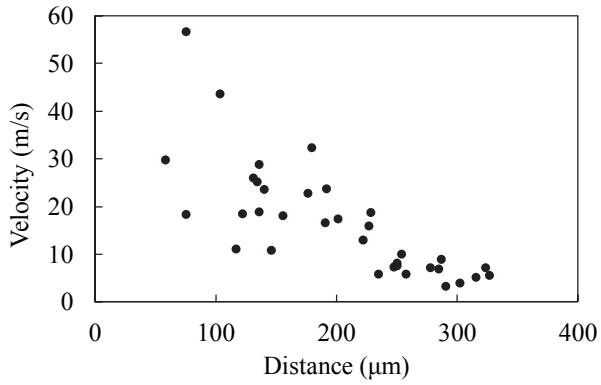

Fig. 7. Moving velocity of the residual bubbles against the distance between the center position of bubbles and the needle electrode at t = 0.5 μs. The data was sampled from three different discharges.

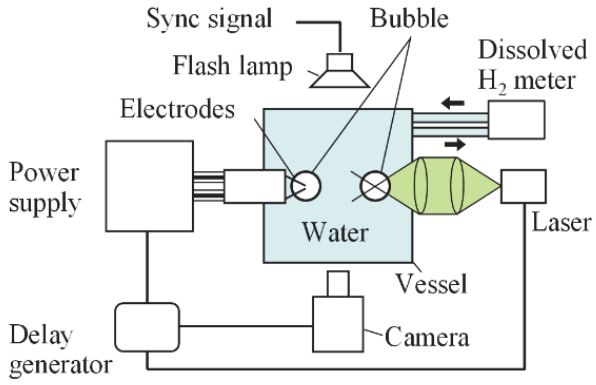

Fig. 8. Schematic of the experimental setup for observation of bubble dynamics and measurement of dissolved hydrogen [22].

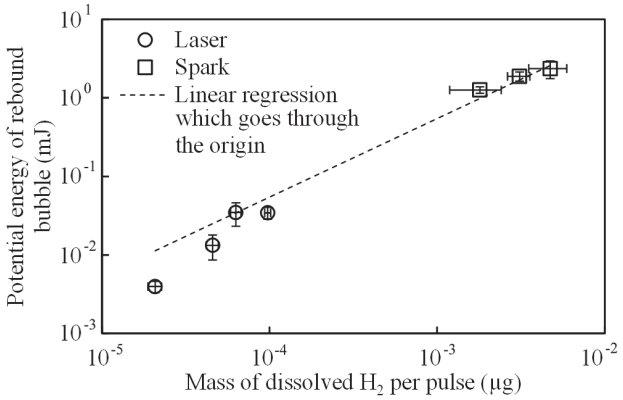

Fig. 9. Potential energy of rebound bubbles against mass of dissolved hydrogen [22].

maximum velocity of 58 m/s, as shown in Fig. 7. The amount of charge of a bubble is estimated by using the following equation.

$$m\frac{dv}{dt} = qE - 6\pi\mu rv \qquad (1)$$

Here, m is the mass of the bubble (1.0×10^{-22} kg), v is the moving velocity of the bubble (57 m/s), r is the radius of the bubble (5 μm), E is the electric field strength (1.29 MV/cm), and μ is the coefficient of viscosity of the water (1 mPa·s). Thus, the amount of charge of the bubble q can be estimated as -4.2×10^{-14} C. This result satisfies the above-mentioned condition, that is, the negative charge.

V. Hydrogen Gas in Plasma-Induced Bubbles

Plasma-generated bubbles remained for some time, but disappeared immediately when the component of gas was the water vapor due to condensation. We focused on hydrogen gas as a non-condensable gas because it is not dissolved in water before plasma generation. To detect the hydrogen gas in a plasma-generated bubble, the dynamics of laser- and spark-induced bubble and dissolved hydrogen gas concentration were clarified using the experimental setup shown in Fig. 8.

Fig. 9 shows the potential energy of a rebound bubble versus the mass of dissolved H_2 per pulse in the cases of the laser and the spark. The potential energy of the rebound bubble increased linearly with an increase in generated hydrogen gas. This result shows that there is a universal relationship between the potential energy of rebound bubbles and the mass of dissolved H_2, and provides further evidence of the effect of hydrogen gas on cavitation bubble dynamics [22]. Furthermore, plasma in water generated emission lines of OH and H, and decreased the oxidation-reduction potential although the pH and conductivity were not significantly changed [22].

VI. Method for Distinguishing Between Gas Bubbles and Solid Particles

Ultrafine bubbles have potential medical and environmental treatments. However, those bubbles cannot be distinguished from gas bubbles and solid particles by conventional methods. To solve this problem, we developed ultra-fine bubbles, a method to distinguish between gas bubbles, and solid particles.

Fig. 10 shows the schematic of the experimental setup. It consisted of a Nd:YAG nano-pulse laser for the generation of a shockwave, a focusing optical system, a water vessel, a high speed camera of 200 Mfps (maximum), a microscope lens, and a Nd:YAG continuous laser for a back light. The nano-pulse laser was focused at the center of the water vessel. A pressure

sensor was set to measure the pressure of the compression and expansion waves. The expansion wave was generated by reflection of a laser-induced shock wave at the water surface, because there is a significant difference between the acoustic impedances of water and air. The acoustic impedance of water is $Z_w = 1.5 \times 10^6$ kg/m^2·s, and that of air is $Z_a = 4.3 \times 10^2$ kg/m^2·s.

From these values, the reflectance of the pressure can be estimated as

$$R_p = (Z_w - Z_a)/(Z_w + Z_a) = -0.99 \quad (2)$$

leading expansion wave accompanying negative pressure by the reflection at the water surface [23].

The stable micro bubbles were generated using ultrasound contrast agents (UCA), which can form bubbles of 2 – 3 μm in diameter. The bubble size distribution was also measured by a laser scattering method. Acrylic particles of 5 μm in diameter were used as solid particles, because they are spherical, of uniform size, and the diameter is close to that of micro bubbles.

Fig. 11 shows the visualization of water after passing the expansion wave at approximately 3 μs after the initial shock wave was generated. Here, (a) is the case of ultrapure water without addition of bubbles or particles, and (b1) and (b2) are the cases of addition of micro bubbles with the UCA densities of 0.92 μg/ml and 9.2 μg/ml, respectively. Further, (c1), (c2), and (c3) are the cases of addition of acrylic particles with densities of 0.88 μg/ml, 8.8 μg/ml, and 88 μg/ml, respectively.

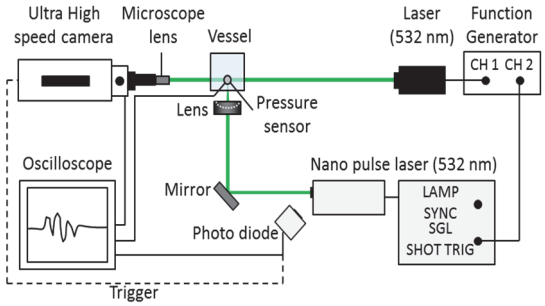

Fig. 10. Schematic of experimental setup for observing growth of cavitation bubbles by application of the expansion wave for the micro bubbles and acrylic particles.

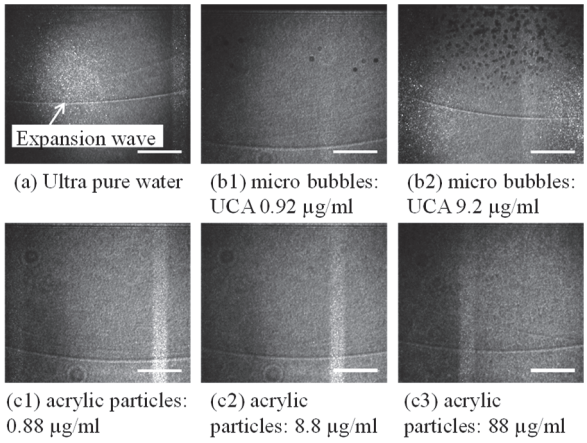

Fig. 11. Visualization of water after passing the expansion wave. Bubble growth was observed only in the case of micro bubbles [23]. The scale bar is 500 μm.

After passing the expansion wave, bubble growth was only observed in the case of micro bubbles (b1) and (b2). The number of visualized bubbles increased with time, and achieved a maximum value at approximately 5–7 μs. However, no bubble was observed in the case of ultrapure water (a) and acrylic particles (c1)–(c3). This result implies that an adequate negative pressure is able to identify between gas bubbles and solid particles [24].

VII. Conclusion

This work introduces the formation of fine bubbles, growth and collapse of streamer channels, charge estimation of plasma fine bubbles, use of hydrogen gas in plasma-induced bubbles, and a method for distinguishing between gas bubbles and solid particles with additional new results.

Acknowledgment

This study was supported by JSPS KAKENHI (grant numbers 16H02311, 15K13864, 25630045, 24246034 and 24108004), the Collaborative Research Project of the Institute of Fluid Science, Tohoku University, Japan, and the Hirayama Manufacturing Corp, with whom collaborative research was conducted.

References

[1] J. S. Haldane, J. G. Priestley, *Respiration* (Oxford, Clarendon, 1935.
[2] R. S. J. Sparks, *J. Volcanol. Geotherm. Res*., 3, 1-37, 1978.
[3] M. S. Plesset, *J. Appl. Mech.*, 16, 277-282, 1949.
[4] R. Parmar, S.K. Majumder, *Chem. Eng. Process.*, 64, 79-97, 2013.
[5] D. Obreschkow, P. Kobel, N. Dorsaz, A. de Bosset, C. Nicollier and M. Farhat, *Phys. Rev. Lett.*, 97, 094502, 2006.
[6] H. Yui and T. Sawada, *Phys. Rev. Lett.*, 85, 3512, 2000.
[7] B. R. Locke, S. M. Thagard, *Plasma Chem. Plasma Process.*, 32, 875–917, 2012.
[8] K. Sato, K. Yasuoka, S. Ishii, *Electric. Eng. Jpn.*, 170, 1-7 (2010).
[9] K. Shimizu, S. Muramatsu, T. Sonoda, M. Blajan, *Int. J. Plasma Environ. Sci. & Tech*., 4, 58-64, 2010.
[10] H. Sönnergren, "Electrosurgical plasma-mediated ablation for application in dermal wound and cartilage debridement," University of Gothenburg, Gothenburg, Sweden, 2015.
[11] L. Enochson, H. Sönnergren, V. Mandalia, A. Lindahl, *Arthroscopy: The Journal of Arthroscopic and Related Surgery*, 28, 1275-1282, 2012.
[12] P. Gautama, H. Toyota, Y. Iwamoto, X. Zhua, S. Nomura, S. Mukasa, *Precision Eng*., 49, 412–420, 2017.
[13] K. Takahashi, Y. Saito, R. Oikawa, T. Okumura, K. Takaki, T. Fujio, *J. Electrostatics*, 91, 61–69, 2018.
[14] P. Bruggeman *et al*., *Plasma Sources Sci. Technol*., 25, 053002, 2016.
[15] T. Miyahara, M. Oizumi, T. Nakatani, T. Sato, *AIP Advances*, 4, 047115, 2014.
[16] T. Sato, T. Nakatani, T. Miyahara, S. Ochiai, M. Oizumi, H. Fujita, T. Miyazaki, *J. Physics: Conf. Ser.*, 656, 012036, 2015.
[17] T. Sato, T. Miyahara, T. Nakatani, *Proc. AFI/TFI-2012*, 76-77, 2012.
[18] H. Fujita, S. Kanazawa, K. Ohtani, A. Komiya, T. Sato, *J. Appl. Phys.*, 113, 113304, 2013.
[19] H. Fujita, S. Kanazawa, K. Ohtani, A. Komiya, T. Kaneko, T. Sato, *EPL*, 105, 15003, 2014.
[20] H. Fujita, S. Kanazawa, K. Ohtani, A. Komiya, T. Kaneko, T. Sato, *J. Appl. Phys.*, 116, 213301, 2014.
[21] H. Fujita, S. Kanazawa, K. Ohtani, A. Komiya, T. Kaneko, T. Sato, *J. Inst. Electrostat. Jpn.*, 39, 21-26, 2015.
[22] T. Sato, M. Tinguely, M. Oizumi, M. Farhat, *APL*, 102, 074105, 2013.
[23] R. Tachikawa, A. Tsukamoto, K. Nakagawa, T. Arafune, H. Liao, E. Kobayashi, T. Ushida, and I. Sakuma, *Adv. Biomed. Eng.*, 1, 68–73, 2012.
[24] T. Sato, Y. Nagasawa, T. Nakajima, K. Ohtani, T. Miyahara, T. Nakatani, *Proc. AFI-2016*, 2-3, 2016.